

Dimensionality reduction in translational noninvariant wave guides

Khee-Kyun Voo¹

*Department of Communication Engineering, Oriental Institute of Technology,
Taipei county 220, Taiwan*

Abstract

A scheme to reduce translational noninvariant quasi-one-dimensional wave guides into singly or multiply connected one-dimensional (1D) lines is proposed. It is meant to simplify the analysis of wave guides, with the low-energy properties of the guides preserved. Guides comprising uniform-cross-sectional sections and discontinuities such as bends and branching junctions are considered. The uniform sections are treated as 1D lines, and the discontinuities are described by equations sets connecting the wave functions on the lines. The procedures to derive the equations and to solve reduced systems are illustrated by examples, and the scheme is found to apply when the discontinuities are distant and the energy is low. When the scheme applies, it may substantially simplify the analysis of a wave guide, and hence the scheme may find uses in the study of related problems, such as quantum wire networks.

Key words: Wave guide, discontinuity, quantum wire, one-dimensional,
PACS: 43.20.Mv, 73.23.Ad, 73.63.Nm, 84.40.Az

1 Introduction

When a wave propagates with a low energy in a quasi-one-dimensional (Q1D) wave guide with an uniform cross section, the guide is effectively one-dimensional (1D) since only the first transverse mode plays a role. However, when a guide comprises discontinuities such as bends and branching junctions, higher transverse modes come into play at the vicinity of the discontinuities. Therefore, in

* Tel.: +886-2-77380145. fax: +886-2-77387411

Email address: kkvoo@mail.oit.edu.tw (Khee-Kyun Voo).

¹ Supported by the National Science Council of Taiwan under Grant NSC96-2112-M-161-001.

principle, a full-mode or full-wave analysis is required, which means a substantial increase in the amount of calculation and the physics is often obscured. Knowing that the guide is essentially 1D in the uniform sections, such a full-wave analysis for the entire system is actually unnecessary. It is the purpose of this paper to present a scheme to eliminate those redundancies and simplify the calculations, yet have those low-energy properties faithfully preserved.

Historically, there has been a number of schemes related to this purpose. The earliest one was due to Kuhn and dates back to 1949 [1]. Then it was made more well-known by Griffith in 1953 [2], and henceforth it has been called the Griffith boundary condition [3,4,5,6,7,8,9,10,11,12,13,14,15,16]. The scheme contains a set of equations relating the wave functions and their first derivatives on the lines connected to a junction [1,2,3,4,5,6,7,8,9,10,11,12,13,14,15,16]. The equations are simple equations that satisfy the unitarity condition at the junction. The scheme has been intuitively stated and has no undetermined parameters. However, recently it has been pointed out by the author *et al.* [17] that it is not clear what kind of realistic Q1D guides the scheme describes. Later than Kuhn, there was another scheme by Shapiro in 1983 [18]. The scheme starts by an unitary matrix relating the amplitudes of the inward and outward waves [18,19,20]. Though this scheme contains free parameters, it also has not been mentioned how the parameters are related to the guides in realistic spaces.

To the present, approaches to the related problems are belong to either one of the mentioned two categories [1,2,3,4,5,6,7,8,9,10,11,12,13,14,15,16,17,18,19,20]. and a common feature of most of the schemes [1,2,3,4,5,6,7,8,9,10,11,12,13,14,15,16,18,19,20] is that the relation between the reduced systems and the original systems is not addressed, and this hinders the application to the study of realistic systems.

In 2006, the author *et al.* proposed a scheme [17], which has been the first attempt to relate reduced and unreduced systems. The scheme resembles that by Kuhn [1], but has an extra phenomenological term with a tuning parameter. The parameter is to be fixed by a comparison between results from the reduced and unreduced systems. The scheme was shown to be a substantial improvement, and many low-energy transport properties were shown to be captured. But still, it is pointed out later in this paper that this simple phenomenology can be inadequate and a more general scheme is needed.

Section 2 illustrates the derivation of the connecting equations to be used in reduced systems, for two typical component structures — the L-bend and the T-junction. Then in Sec. 3, these two structures are assembled into more elaborated structures, and the wave propagation in the structures are studied in and compared between, the reduced and unreduced systems. In Sec. 4, a few concluding remarks are given.

2 Formulation

The scheme to be proposed can be summarized as in the following. For a particular discontinuity, the scattering matrix (S -matrix) is evaluated using a full-wave treatment, and then the matrix is truncated leaving only those elements relating the first transverse modes in the branch guides. The truncated S -matrix is then used to connect the 1D wave functions in reduced systems.

The two-dimensional (2D) time-independent Schrödinger equation (TISE) $-\hbar^2/(2m_0)[\partial_x^2\Psi + \partial_y^2\Psi] + V(x, y)\Psi = E\Psi$, with $V(x, y) = 0$ and hard wall boundaries is considered. For a wave with an energy E in a guide having a width W , the wave function can be written as a sum of direct products of transverse modes and longitudinal waves. Labeling the guide by η and defining a coordinate system (x_η, y_η) in the guide, where x_η is in the longitudinal direction and y_η is in the transverse direction ($0 < y_\eta < W$), the wave function can be written as

$$\begin{aligned} \Psi_\eta(E; x_\eta, y_\eta) = & \sum_{m=1}^{N_\eta} \sqrt{\frac{2}{W}} \sin\left(\frac{m\pi y_\eta}{W}\right) \\ & \times \left(A_\eta^{(m)} e^{ik^{(m)}x_\eta} + B_\eta^{(m)} e^{-ik^{(m)}x_\eta} \right), \end{aligned} \quad (1)$$

where $k^{(m)} \equiv \sqrt{2m_0E/\hbar^2 - (m\pi/W)^2}$ is the longitudinal wave number for the m -th transverse mode, which can be propagating or evanescent, and N_η is a large enough integer. In a 1D space, the TISE becomes $-\hbar^2/(2m_0)\partial_x^2\psi + V(x)\psi = E\psi$. For a line labeled by η , and with a coordinate x_η defined on it, the wave function for $V(x) = 0$ is

$$\psi_\eta(E; x_\eta, y_\eta) = A_\eta e^{ikx_\eta} + B_\eta e^{-ikx_\eta}, \quad (2)$$

where k is the longitudinal wave number given by $k = \sqrt{2m_0E}/\hbar$. When results from 2D guides and 1D lines are compared, $A_\eta^{(1)}$ ($B_\eta^{(1)}$) is compared with A_η (B_η), and $k^{(1)}$ is compared with k .

Two discontinuities in 2D wave guides are considered, the L-bend and T-junction as shown in Fig. 1(a) and 1(b) respectively. The discontinuities are divided into regions which are labeled by 1, 2, 3, and D in our discussion. Coordinates are also defined in the branch guides, and wave functions in the branch guides are in the form given by Eq. (1). The S -matrices are to be presented in terms of these coordinates. The symbols used to denote the L-bend and T-junction in reduced systems are shown in Fig. 1(c) and 1(d) respectively.

We only sketch the evaluation of the S -matrices here, since the techniques are

well-established and are detailed in the literatures [21,22]. The wave function in region D [see Figs. 1(a) and 1(b)] is also expanded in terms of undetermined amplitudes, and they are connected to wave functions in other regions by the conditions of continuities of wave functions and normal derivatives of wave functions at the boundaries between the regions. Otherwise, one may also solve the TISE in a discretized space, where the TISE is a set of finite-difference (FD) equations.

For the T-junction shown in Fig. 1(b), we can get an equation for the amplitudes of the waves in the branch guides (regions 1, 2, and 3) such as

$$\begin{bmatrix} B_1^{(1)} \\ B_2^{(1)} \\ B_3^{(1)} \\ \dots \end{bmatrix} = \begin{bmatrix} s_{11}^T & s_{12}^T & s_{13}^T & \dots \\ s_{21}^T & s_{22}^T & s_{23}^T & \dots \\ s_{31}^T & s_{32}^T & s_{33}^T & \dots \\ \dots & \dots & \dots & \dots \end{bmatrix} \begin{bmatrix} A_1^{(1)} \\ A_2^{(1)} \\ A_3^{(1)} \\ \dots \end{bmatrix}, \quad (3)$$

where $A_\eta^{(m)}$ ($B_\eta^{(m)}$) is an amplitude for an inward (outward) wave in Eq. (1). Truncating the matrices in Eq. (3) and retaining only terms related to the first transverse modes in the branch guides, we get

$$\begin{bmatrix} B_1 \\ B_2 \\ B_3 \end{bmatrix} = S_T \begin{bmatrix} A_1 \\ A_2 \\ A_3 \end{bmatrix}, \quad (4)$$

where A_η and B_η , $\eta = 1, 2$, and 3 are amplitudes in Eq. (2), and

$$S_T = \begin{bmatrix} s_{11}^T & s_{12}^T & s_{13}^T \\ s_{21}^T & s_{22}^T & s_{23}^T \\ s_{31}^T & s_{32}^T & s_{33}^T \end{bmatrix}, \quad (5)$$

where the coordinates are chosen as toward the junction, and $x_1 = x_2 = x_3 = 0$ at the junction as shown in Fig. 1(d). For the scheme to work, it is necessary that the energy is such that only the first transverse mode is propagating, and the exponential tails of the evanescent waves of higher modes emanated from the discontinuities are shorter than the distances between the discontinuities.

We can also write Eq. (4) in terms of ψ_η . Using $A_\eta = [\psi_\eta + d\psi_\eta/d(ikx_\eta)]/2$ and $B_\eta = [\psi_\eta - d\psi_\eta/d(ikx_\eta)]/2$ at $x_\eta = 0$, the connecting equation can be rewritten as

$$\frac{1 + S_T}{ik} \begin{bmatrix} \frac{d\psi_1}{dx_1} \\ \frac{d\psi_2}{dx_2} \\ \frac{d\psi_3}{dx_3} \end{bmatrix} = (1 - S_T) \begin{bmatrix} \psi_1 \\ \psi_2 \\ \psi_3 \end{bmatrix}, \quad (6)$$

where the wave functions and their derivatives are evaluated at the discontinuity, and the directions of the coordinates are defined to be toward the discontinuity. Note that in Eq. (6), it is not necessary that the origins of the coordinates be located at the discontinuity.

Likewise, the connecting equation for the L-bend shown in Fig. 1(a) can be written as

$$\frac{1 + S_L}{ik} \begin{bmatrix} \frac{d\psi_1}{dx_1} \\ \frac{d\psi_2}{dx_2} \end{bmatrix} = (1 - S_L) \begin{bmatrix} \psi_1 \\ \psi_2 \end{bmatrix}, \quad (7)$$

where the directions of the coordinates are defined to be toward the discontinuity as shown in Fig. 1(c).

Note that, the S -matrices are symmetric ($S_L^t = S_L$ and $S_T^t = S_T$) and unitary ($S_L^\dagger S_L = 1$ and $S_T^\dagger S_T = 1$). The unitarity implies $\sum_\eta (|A_\eta|^2 - |B_\eta|^2) = 0$, and since $A_\eta = [\psi_\eta + d\psi_\eta/d(ikx_\eta)]/[2e^{ikx_\eta}]$ and $B_\eta = [\psi_\eta - d\psi_\eta/d(ikx_\eta)]/[2e^{-ikx_\eta}]$, the unitarity can be rephrased as a more intuitive equality $\sum_\eta \psi_\eta^* d\psi_\eta/d(ikx_\eta) = 0$, or there is no net inflow of probability current to the discontinuity.

The numerical results for the magnitudes and arguments of the elements of S_L are plotted in Figs. 2(a) and 2(b) respectively, and the results for S_T are plotted in Figs. 2(c) and 2(d) respectively, versus a dimensionless longitudinal wave number κ defined by $\kappa \equiv k^{(1)}W/\pi$. For the reference of the readers, the cutoff of the second transverse mode is at $\kappa = \sqrt{3} \simeq 1.73$. The results are obtained using discretized spaces with 20 sites across a width of W , and they are found to be in congruence with results from 10 sites within windows of $\Delta\kappa \simeq 0.02$ on the horizontal axes, and windows of $\Delta|S| \simeq 0.02$ and $\Delta[\pi^{-1}\text{Arg}(S)] \simeq 0.005$ on the vertical axes, which implies that the continuous space limit has been approached.

Since the L-bend and T-junction appear quite often in practical problems, it may be convenient to have their S -matrices in analytic forms. Within a finite range of κ , it is possible to approximate a S -matrix by analytic functions. For the S_L at $\kappa < 1$, we may approximate the magnitudes and arguments of the elements by

$$|(S_L)_{11}| \simeq \frac{1}{1 + (2.796\kappa - 1.498\kappa^2)^2}, \quad (8)$$

$$\text{Arg } (S_L)_{11} \simeq (1 - 0.586\kappa + 1.496\kappa^2 - 0.541\kappa^3)\pi, \quad (9)$$

$$|(S_L)_{12}| = \sqrt{1 - |(S_L)_{11}|^2}, \quad (10)$$

$$\text{Arg } (S_L)_{12} = \text{Arg } (S_L)_{11} - \frac{\pi}{2}, \quad (11)$$

$$(S_L)_{21} = (S_L)_{12}, \quad \text{and} \quad (12)$$

$$(S_L)_{22} = (S_L)_{11}. \quad (13)$$

Within $\kappa < 1$, the approximation for $|(S_L)_{11}|$ in Eq. (8) and the approximation for $\text{Arg } (S_L)_{11}$ in Eq. (9) approximate the numerical results in Figs. 2(a) and 2(b) respectively up to $\Delta|S| < 0.01$ and $\Delta[\pi^{-1}\text{Arg}(S)] < 0.01$ accuracy. The exact equalities Eqs. (10)-(13) are due to the symmetry and unitarity of the S -matrix and the exchange of leads 1 and 2.

For the S_T at $\kappa < 1$, it is found that the numerical results for the elements can be approximated by

$$|(S_T)_{11}| \simeq \frac{1}{1 + (1.734\kappa - 0.808\kappa^2)^2}, \quad (14)$$

$$\text{Arg } (S_T)_{11} \simeq (1 - 0.051\kappa + 0.559\kappa^2 + 0.018\kappa^3)\pi, \quad (15)$$

$$|(S_T)_{12}| = \sqrt{\frac{1 - |(S_T)_{11}|^2}{2}}, \quad (16)$$

$$\text{Arg } (S_T)_{12} \simeq \left(\frac{1}{2} - 0.153\kappa + 0.585\kappa^2 - 0.087\kappa^3\right)\pi, \quad (17)$$

$$(S_T)_{13} = (S_T)_{12}, \quad (18)$$

$$|(S_T)_{22}| \simeq \frac{1}{1 + (1.780\kappa + 0.015\kappa^2)^2}, \quad (19)$$

$$\text{Arg } (S_T)_{22} \simeq (1 + 0.415\kappa + 0.508\kappa^2 + 0.089\kappa^3)\pi, \quad (20)$$

$$|(S_T)_{23}| = \sqrt{\frac{1 + |(S_T)_{11}|^2}{2} - |(S_T)_{22}|^2}, \quad (21)$$

$$\text{Arg } (S_T)_{23} \simeq \left(\frac{1}{2} + 0.205\kappa + 0.616\kappa^2 - 0.202\kappa^3\right)\pi, \quad (22)$$

$$(S_T)_{33} = (S_T)_{22}, \quad \text{and} \quad (23)$$

$$S_T^\dagger = S_T. \quad (24)$$

For $\kappa < 1$, the above approximations for $|S|$ and $\text{Arg } (S)$ approximate the results in Figs. 2(c) and 2(d) respectively up to $\Delta|S| < 0.01$ and $\Delta[\pi^{-1}\text{Arg}(S)] < 0.01$ accuracy. The exact equalities are due to the symmetry and unitarity of the S -matrix, and the exchange of leads 2 and 3.

3 Comparison between reduced and unreduced systems

In this section, three wave guides which are composites of the discussed L-bend and T-junction are analyzed. The scattering amplitudes from the original 2D structures and the reduced multiply-connected 1D structures are compared. Cases of far apart and close discontinuities, different orientations of guides, and straight and smoothly curved guides are considered.

The first example is a 2D square loop resonator with two leads as depicted in Fig. 3(a). The translational invariant sections have the same width W . For simplicity, the distances between the discontinuities are chosen to be the same, and are denoted by d as shown. In Fig. 3(b), a reduced version for the structure in Fig. 3(a) is shown. The magnitude of the transmission scattering amplitude $|S_{12}|$ has been plotted versus κ for the unreduced and reduced systems, in Figs. 3(c) and 3(d), for $d = 4W$ and $d = 0.1W$ respectively. The S_{12} for the 2D structure is the scattering amplitude from the first transverse mode in lead 2 to the first transverse mode in lead 1, and the dimensionless wave number κ is now defined by $\kappa \equiv k^{(1)}W/\pi$ or $\kappa \equiv kW/\pi$ depending on the context. The procedure for a full-wave evaluation of $|S_{12}|$ for the 2D structure is standard [21,22] and it is not to be repeated here, but only the result is given. The result here is obtained with a FD TISE, and the number of sites across a width W is equal to 20.

In the reduced system shown in Fig. 3(b), a line labeled by η and given a coordinate x_η has a wave function in the form given in Eq. (2). For the coordinates defined in Fig. 3(b), the wave functions on the lines are connected by

$$\frac{1 + S_L}{ik} \begin{bmatrix} \frac{d\psi_3}{dx_3} \Big|_{x_3=d} \\ -\frac{d\psi_4}{dx_4} \Big|_{x_4=0} \end{bmatrix} = (1 - S_L) \begin{bmatrix} \psi_3|_{x_3=d} \\ \psi_4|_{x_4=0} \end{bmatrix}, \quad (25)$$

$$\frac{1 + S_L}{ik} \begin{bmatrix} \frac{d\psi_4}{dx_4} \Big|_{x_4=d} \\ -\frac{d\psi_5}{dx_5} \Big|_{x_5=0} \end{bmatrix} = (1 - S_L) \begin{bmatrix} \psi_4|_{x_4=d} \\ \psi_5|_{x_5=0} \end{bmatrix}, \quad (26)$$

$$\frac{1 + S_T}{ik} \begin{bmatrix} -\frac{d\psi_3}{dx_3} \Big|_{x_3=0} \\ \frac{d\psi_1}{dx_1} \Big|_{x_1=0} \\ \frac{d\psi_6}{dx_6} \Big|_{x_6=d} \end{bmatrix} = (1 - S_T) \begin{bmatrix} \psi_3|_{x_3=0} \\ \psi_1|_{x_1=0} \\ \psi_6|_{x_6=d} \end{bmatrix}, \quad (27)$$

and

$$\frac{1 + S_T}{ik} \begin{bmatrix} \frac{d\psi_5}{dx_5} \Big|_{x_5=d} \\ \frac{d\psi_2}{dx_2} \Big|_{x_2=0} \\ -\frac{d\psi_6}{dx_6} \Big|_{x_6=0} \end{bmatrix} = (1 - S_T) \begin{bmatrix} \psi_5|_{x_5=d} \\ \psi_2|_{x_2=0} \\ \psi_6|_{x_6=0} \end{bmatrix}. \quad (28)$$

This contains 10 equations with 10 unknowns, when A_1 and A_2 are given. The scattering amplitude S_{12} is obtained as $S_{12} = B_1$ at $A_1 = 0$ and $A_2 = 1$. The magnitude $|S_{12}|$ is plotted in Figs. 3(c) and 3(d), for values of d corresponding to the original 2D structure. In the calculation, S_L and S_T use the numerical values shown in Fig. 2.

In the case of $d = 4W$ [see Fig. 3(c)], results from the original 2D and the reduced systems are nearly indistinguishable when seen in the size of the plot, while in the case of $d = 0.1W$ [see Fig. 3(d)], the two results have a perceptible difference, especially when κ becomes large. A criterion for the applicability of the one-mode reduction scheme is $|k^{(2)}d| \gg 1$, which means that the exponential tails of the evanescent waves for the higher transverse modes emanating from the discontinuities, is much shorter than the distances between the discontinuities. In this regime, the evanescent waves from neighboring discontinuities do not overlap each other, and the discontinuities communicate with each other only via the first transverse modes in the translational invariant sections. Hence, the higher transverse modes in the sections are redundant, and a single-mode description is adequate.

The length of an exponential tail of the second transverse mode is of the order of $|k^{(2)}|^{-1}$. The values of $|k^{(2)}W|^{-1}$ are approximately equal to 0.18 ($\kappa = 0$), 0.23 ($\kappa = 1.0$), 0.28 ($\kappa = 1.3$), 0.37 ($\kappa = 1.5$), 0.48 ($\kappa = 1.6$), 0.96 ($\kappa = 1.7$), and 1.56 ($\kappa = 1.72$), for the values of κ given in the brackets [23]. It is seen that $|k^{(2)}W|^{-1}$ becomes large only when κ approaches $\sqrt{3}$. For $d = 4W$, $|k^{(2)}d| \simeq 14 \gg 1$ at $\kappa = 1.3$, and that justifies the reduction scheme in the entire range of κ in Fig. 3(c) [and also Fig. 4(c) later in this section]. For $d = 0.1W$, $|k^{(2)}d| \simeq 0.54$ at $\kappa = 0$, and $|k^{(2)}d|$ is certainly not “large” for Fig. 3(d) [and also Fig. 4(d) later in this section]. In spite of this, the scheme might still perform up to certain precision, until it really starts to breakdown at $\kappa \sim 1.2$ as seen in Fig. 3(d) [see also Fig. 4(d)]. However, its reliability in this regime of κ is uncontrolled in general.

Another 2D wave guide as shown in Fig. 4(a) is also analyzed. This structure resembles the one in Fig. 3(a), except that one of the leads is rotated by 90-degree. The width of the uniform sections are also denoted by W , and

the distances between the discontinuities are also denoted by d . A reduced structure for the guide is shown in Fig. 4(b), and the magnitude of the transmission scattering amplitude $|S_{12}|$ is also plotted for both of the reduced and unreduced structures in Figs. 4(c) [for $d = 4W$] and 4(d) [for $d = 0.1W$].

The connecting equations for the reduced structure in Fig. 4(b) are Eqs. (25), (26), (27), and

$$\frac{1 + S_T}{ik} \begin{bmatrix} -\frac{d\psi_6}{dx_6} \Big|_{x_6=0} \\ \frac{d\psi_2}{dx_2} \Big|_{x_2=0} \\ \frac{d\psi_5}{dx_5} \Big|_{x_5=d} \end{bmatrix} = (1 - S_T) \begin{bmatrix} \psi_6|_{x_6=0} \\ \psi_2|_{x_2=0} \\ \psi_5|_{x_5=d} \end{bmatrix}. \quad (29)$$

The transmission scattering amplitude S_{12} is found as in the previous example. Likewise, it is seen in Fig. 4(c) that the reduction scheme is guaranteed to work in the $|k^{(2)}d| \gg 1$ regime. Also, it is seen in Fig. 4(d) that the scheme might still work qualitatively or semi-quantitatively, when κ is departed from this regime.

Comparing the result in Fig. 3(c) with that in Fig. 4(c), and the result in Fig. 3(d) with that in Fig. 4(d), it is seen that scattering amplitudes can depend significantly on the orientations of the branch guides at a discontinuity. This indicates that reduction schemes with symmetric branch lines such as those in Refs. [1,2,3,17] are not adequate for some cases.

The third example is a 2D annulus structure with an inner and an outer radii of $R - W/2$ and $R + W/2$ respectively, and two mutually perpendicular leads of width W radially connected to the annulus as shown in Fig. 5(a). Figure 5(b) shows a reduced version of it. For the 2D annulus, we may follow a mode-matching full-wave treatment formulated by Xia and Li [24]. In the annulus the wave function $\Psi_{\text{ann.}}$ can be expanded by radial and angular modes, $\Psi_{\text{ann.}}(r, \theta) = \sum_{l=-M}^M \phi_l(Kr) e^{il\theta}$, where a radial mode is given by $\phi_l(Kr) \equiv a_l J_l(Kr) + b_l Y_l(Kr)$, and $K = \sqrt{2m_0 E}/\hbar$. The r and θ are the radial and angular coordinates respectively; and the J_l and Y_l are the Bessel functions of the first and second kinds respectively. At the inner radius, $\phi_l|_{r=R-W/2} = 0$ for any θ ; At the outer radius, $\Psi_{\text{ann.}}|_{r=R+W/2} = 0$ when θ is away from the leads, and $\Psi_{\text{ann.}}|_{r=R+W/2} = \Psi_\eta$, when θ is in the range of lead η . In addition, the radial derivative $\partial\Psi_{\text{ann.}}/\partial r$ is equated with the longitudinal derivative $\partial\Psi_\eta/\partial x_\eta$ when $\Psi_{\text{ann.}}$ and Ψ_η meet at the outer arc of the annulus. The difference between the straight transverse cuts of the leads and the outer arcs of the annulus is neglected. The wave functions in the leads and the annulus are hence matched, and one can get a set of equations relating the coefficients of the modes in

the different regions. The transmission scattering amplitude $|S_{12}|$ for the 2D annulus is plotted for $R = 3W$ [Fig. 5(c)] and $R = 0.8W$ [Fig. 5(d)].

To apply a reduced calculation to the reduced system in Fig. 5(b), note that for smoothly curved guides with small curvatures, the back-scattering is small and the guides can be treated as reflectionless for most purposes. Guides with constant curvatures are translational invariant and indeed reflectionless, though the lengths and widths may not be rigorously defined. The junctions are treated as T-junctions. For the left junction,

$$\frac{1 + S_T}{ik} \begin{bmatrix} \left. \frac{d\psi_1}{dx_1} \right|_{x_1=0} \\ - \left. \frac{d\psi_3}{dx_3} \right|_{x_3=0} \\ \left. \frac{d\psi_4}{dx_4} \right|_{x_4=d_4} \end{bmatrix} = (1 - S_T) \begin{bmatrix} \psi_1|_{x_1=0} \\ \psi_3|_{x_3=0} \\ \psi_4|_{x_4=d_4} \end{bmatrix}; \quad (30)$$

for the right junction,

$$\frac{1 + S_T}{ik} \begin{bmatrix} \left. \frac{d\psi_2}{dx_2} \right|_{x_2=0} \\ \left. \frac{d\psi_3}{dx_3} \right|_{x_3=d_3} \\ - \left. \frac{d\psi_4}{dx_4} \right|_{x_4=0} \end{bmatrix} = (1 - S_T) \begin{bmatrix} \psi_2|_{x_2=0} \\ \psi_3|_{x_3=d_3} \\ \psi_4|_{x_4=0} \end{bmatrix}. \quad (31)$$

We let $d_\eta = R\theta_\eta - W$, where $\theta_3 = 3\pi/2$ and $\theta_4 = \pi/2$, and the subtraction is to approximately exclude the regions in the junctions [see region D in Fig. 1(b)]. The radius $R = 3W$ gives $d_3 \simeq 13.1W$ and $d_4 \simeq 3.7W$, and $R = 0.8W$ gives $d_3 \simeq 2.77W$ and $d_4 \simeq 0.26W$. Results for $|S_{12}|$ are plotted in Figs. 5(c) and 5(d).

If one analyzes the reduced system using the Griffith scheme [1,2,3,6] for a junction with three branches, the left junction has

$$\psi_1|_{x_1=0} = \psi_3|_{x_3=0} = \psi_4|_{x_4=d_4} \quad \text{and} \quad (32)$$

$$\left. \frac{d\psi_1}{dx_1} \right|_{x_1=0} - \left. \frac{d\psi_3}{dx_3} \right|_{x_3=0} + \left. \frac{d\psi_4}{dx_4} \right|_{x_4=d_4} = 0, \quad (33)$$

and the right junction has

$$\psi_2|_{x_2=0} = \psi_3|_{x_3=d_3} = \psi_4|_{x_4=0} \quad \text{and} \quad (34)$$

$$\left. \frac{d\psi_2}{dx_2} \right|_{x_2=0} + \left. \frac{d\psi_3}{dx_3} \right|_{x_3=d_3} - \left. \frac{d\psi_4}{dx_4} \right|_{x_4=0} = 0. \quad (35)$$

Note that the equations at a junction are symmetric with respect to an interchange of any two branches. Using the same d_3 and d_4 , results for $|S_{12}|$ are also plotted in Figs. 5(c) and 5(d). Comparing the results from our scheme and the Griffith scheme with the result from the 2D calculation, it is seen that the Griffith result is qualitatively different from the 2D result in general, while our scheme captures the essential features in the 2D result, especially in the case of longer guide sections [Fig. 5(c)].

The lengths of the guide sections in Fig. 5 are about the sizes of those in Figs. 3 and 4, but the disagreement between the 2D and reduced calculation results are seen to be more severe in Fig. 5, especially in the case of short guide sections [Fig. 5(d)]. This is mainly due to vaguer notions of the lengths and widths of the guide sections between the discontinuities, and a stronger distortion of the shapes of the junctions from a “T” [Fig. 1(b)], when the guide sections are curved and short, in addition to a violation of the criterion $|k^{(2)}d| \gg 1$. Comparing Figs. 5(c) and 5(d), it is also seen that our scheme performs better when the discontinuities are more apart.

4 Concluding Remarks

This study has shown that the higher transverse modes in the uniform-cross-sectional sections in wave guides can give only a minor effect on the low-energy properties of the guides. A scheme to remove these modes and a criterion for the energy range ($|k^{(2)}d| \gg 1$) in which the scheme applies have been proposed. In the scheme, a reduced system and its corresponding system in a realistic space have a sound relationship, and therefore the scheme may find more practical use in the analyses of realistic wave guides than previously reported schemes [1,17,18].

The electronic spin degrees of freedom may also be included into the scheme by expanding the current one-mode S -matrices to two-mode S -matrices, for the up and down spin channels, and in the same way as in Sec. 3, the two-mode S -matrices are calibrated by full-wave calculations for systems in realistic spaces. Likewise, the precision of the scheme at short guide sections can also be refined by including more transverse modes and using multi-mode S -matrices.

References

- [1] H. Kuhn, *Helv. Chim. Acta* **32**, 2247 (1949).
- [2] J. Stanley Griffith, *Trans. Faraday Soc.* **49**, 345 (1953); *ibid.*, **49**, 650 (1953).
- [3] K. Ruedenberg and C. W. Scherr, *J. Chem. Phys.* **21**, 1565 (1953).
- [4] P. Exner and P. Seba, *Rep. Math. Phys.* **28**, 7 (1989).
- [5] T. Kottos and U. Smilansky, *Ann. of Phys.* **274**, 76 (1999).
- [6] J.-B. Xia, *Phys. Rev. B* **45**, 3593 (1992).
- [7] J. M. Mao, Y. Huang, and J. M. Zhou, *J. Appl. Phys.* **73**, 1853 (1993).
- [8] P. Singha Deo and A. M. Jayannavar, *Phys. Rev. B* **50**, 11629 (1994).
- [9] M. V. Moskalets, *Low Temp. Phys.* **23**, 824 (1997).
- [10] C.-M. Ryu and S. Y. Cho, *Phys. Rev. B* **58**, 3572 (1998).
- [11] S. Bandopadhyay, P. Singha Deo, and A. M. Jayannavar, *Phys. Rev. B* **70**, 75315 (2004).
- [12] D. Bercioux, M. Governale, V. Cataudella, and V. M. Ramaglia, *Phys. Rev. Lett.* **93**, 56802 (2004).
- [13] P. Foldi, B. Molnar, M. G. Benedict, and F. M. Peeters, *Phys. Rev. B* **71**, 33309 (2005).
- [14] U. Aeberhand, K. Wakabayashi, and M. Sigrist, *Phys. Rev. B* **72**, 75328 (2005).
- [15] X. F. Wang and P. Vasilopoulos, *Phys. Rev. B* **72**, 165336 (2005).
- [16] O. Kalman, P. Foldi, M. G. Benedict, and F. M. Peeters, arXiv:0806.2734 (unpublished).
- [17] K.-K. Voo, S.-C. Chen, C.-S. Tang, and C.-S. Chu, *Phys. Rev. B* **73**, 35307 (2006).
- [18] B. Shapiro, *Phys. Rev. Lett.* **50**, 747 (1983).
- [19] M. Buttiker, Y. Imry, and M. Y. Azbel, *Phys. Rev. A* **30**, 1982 (1984).
- [20] Y. Gefen, Y. Imry, and M. Y. Azbel, *Phys. Rev. Lett.* **52**, 129 (1984).
- [21] S. Datta, *Electronic Transport in Mesoscopic Systems*, 1st Ed. (Cambridge University Press, Cambridge, 1995).
- [22] D. K. Ferry and S. M. Goodnick, *Transport in Nanostructures*, 1st Ed. (Cambridge University Press, Cambridge, 1997).
- [23] $k^{(2)}$ and κ are related by $k^{(2)}W = \pi\sqrt{\kappa^2 - 3}$.
- [24] J.-B. Xia and S.-S. Li, *Phys. Rev. B* **66**, 35311 (2002).

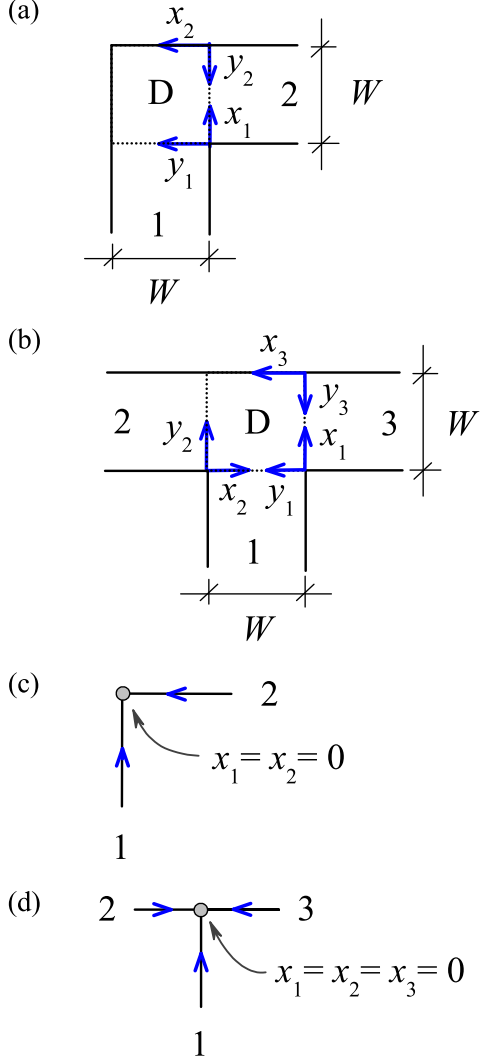


Fig. 1. (Color online) The two discontinuities in 2D wave guides considered in this paper, (a) the L-bend and (b) the T-junction. The widths of the guides are denoted by W . The branch guides are labeled by 1, 2, and 3, in which coordinates are defined as shown. The translational noninvariant regions are labeled by D. In the reduced systems, (c) a L-bend is represented by a “L,” and (d) a T-junction is represented by a “T.” The arrows on the branch lines indicate the positive directions of the coordinates defined on the lines, and the origins of the coordinates are defined to be at the branching nodes.

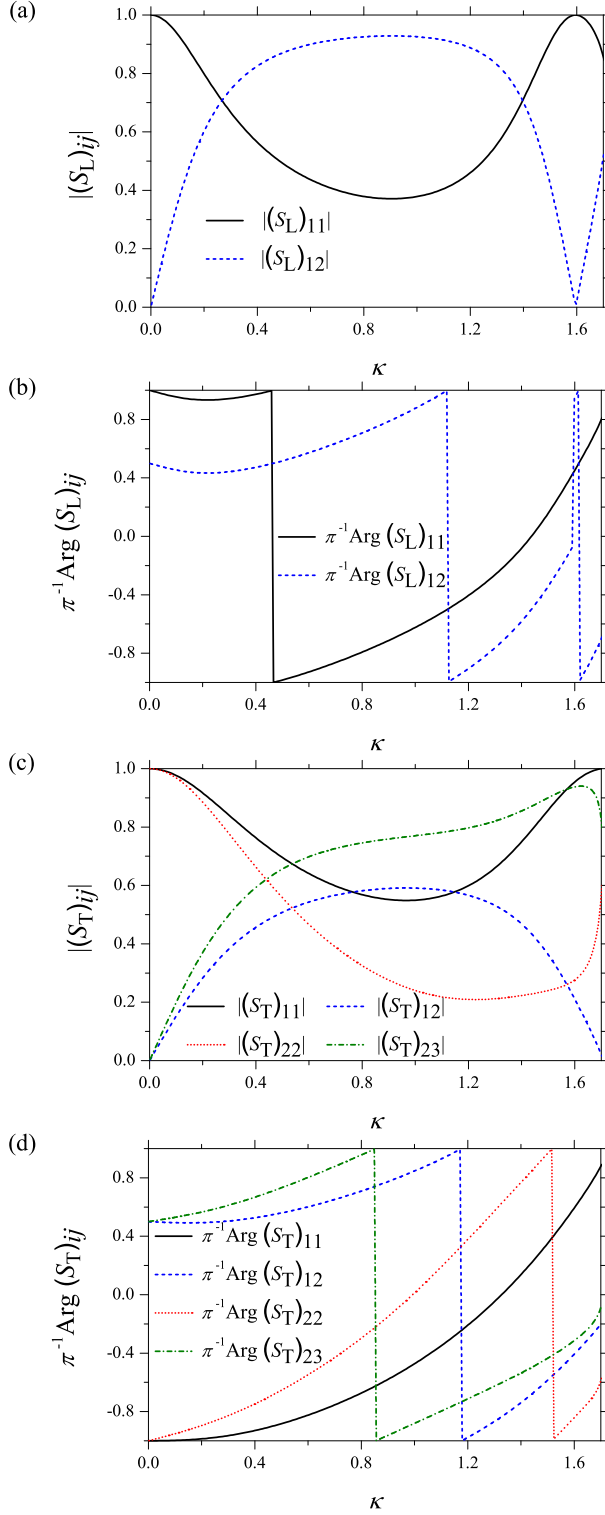


Fig. 2. (Color online) The (a) magnitudes of the elements of S_L , (b) arguments of the elements of S_L , (c) magnitudes of the elements of S_T , and (d) arguments of the elements of S_T are plotted versus a dimensionless longitudinal wave number κ , defined by $\kappa \equiv k^{(1)}W/\pi$.

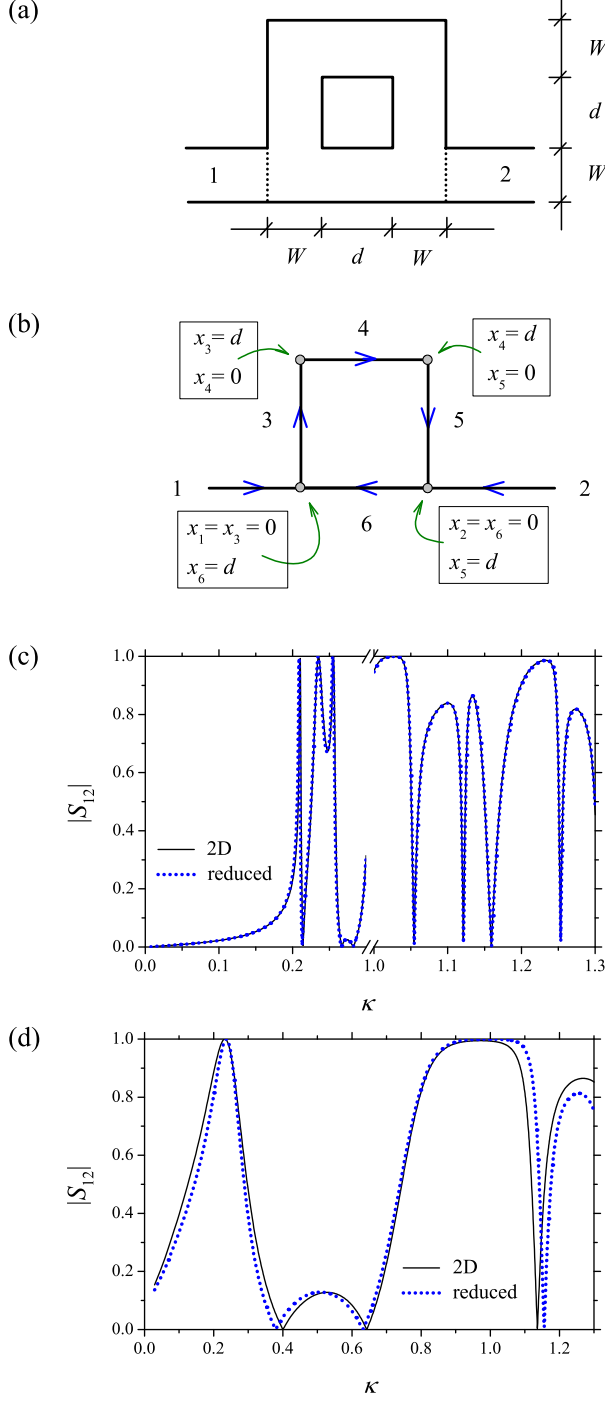


Fig. 3. (Color online) (a) A considered 2D composite structure. The uniform-cross-sectional sections have the same width W . The distances between the discontinuities are chosen to be the same and are denoted by d . (b) A reduced version of the above structure. A coordinate x_η is defined on line η ($\eta = 1 - 6$) with a positive direction indicated by an arrow on the line. The coordinates of the discontinuities on the lines are shown in the boxes. (c) For $d = 4W$, the magnitude of the transmission scattering amplitude $|S_{12}|$ is plotted versus κ , for the original 2D system (solid line) and the reduced system (dotted line). The κ here is defined by $\kappa \equiv k^{(1)}W/\pi$ or $\kappa \equiv kW/\pi$. Seen in the size of the present graph, the two curves are almost indistinguishable. (d) For $d = 0.1W$, results for $|S_{12}|$ are also shown. The curves deviate from each other, especially when κ gets larger.

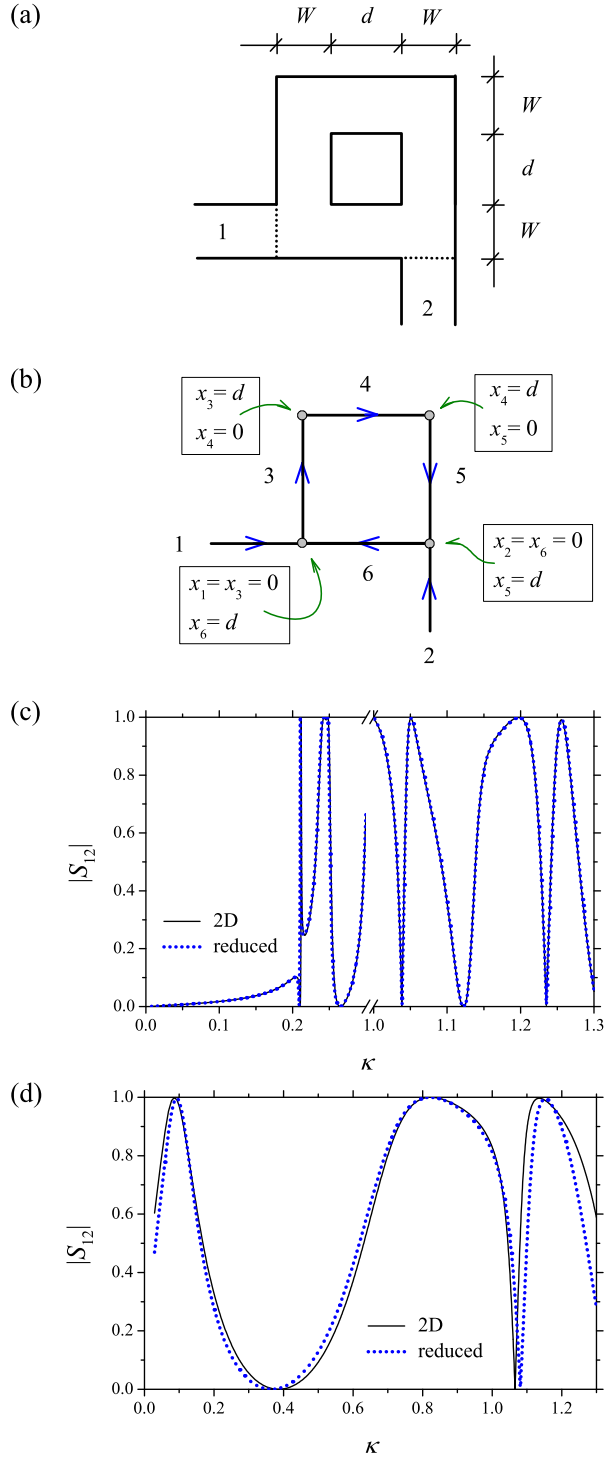


Fig. 4. See the caption in Fig. 3.

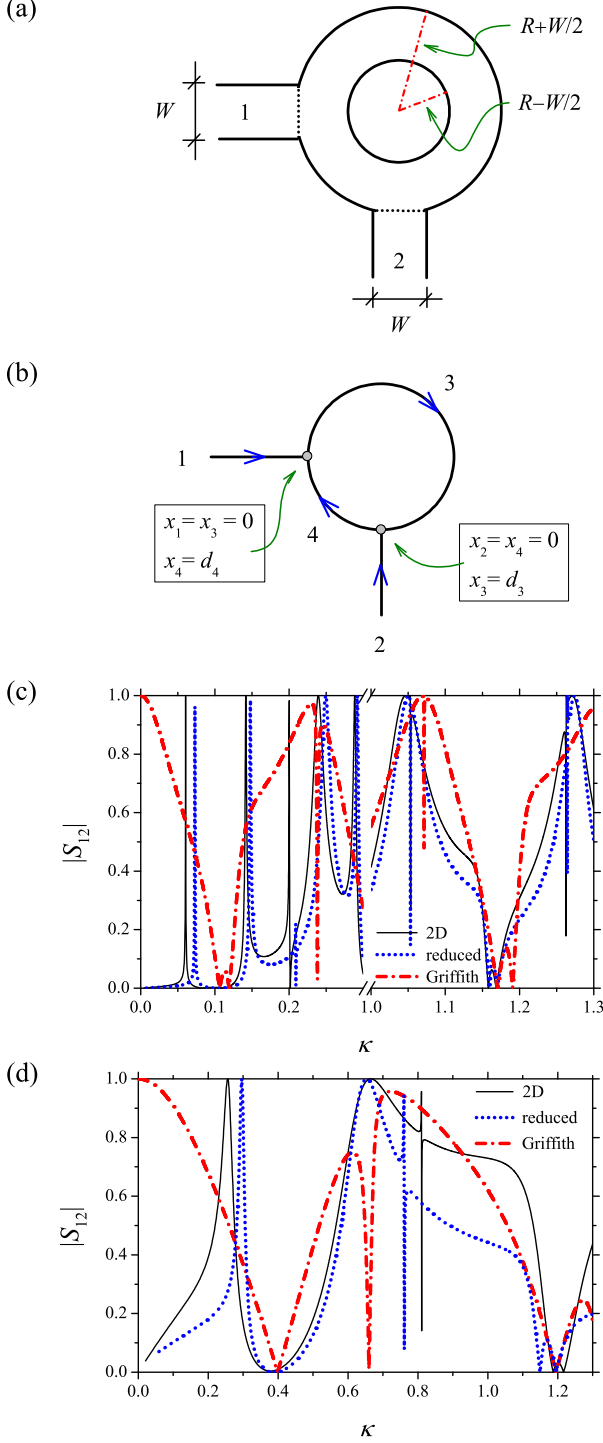


Fig. 5. (Color online) (a) A considered 2D annulus with two mutually perpendicular and radially connected leads. The leads have the same width W . The inner radius $R - W/2$ and outer radius $R + W/2$ of the annulus are defined as shown. (b) A reduced version of the annulus. A coordinate x_η is defined on line η ($\eta = 1 - 4$) with a positive direction indicated by an arrow on the line. The coordinates of the junctions on the lines are shown in the boxes. (c) For $R = 3W$, the magnitude of the transmission scattering amplitude $|S_{12}|$ is plotted versus κ , for the original 2D annulus (solid line) and the reduced system (dotted line for our scheme, and dash-dotted line for the Griffith scheme). The κ here is defined by $\kappa \equiv k^{(1)}W/\pi$ (note that $k^{(1)}$ is defined in the leads) or $\kappa \equiv kW/\pi$. (d) For $R = 0.8W$, results for $|S_{12}|$ are also shown.